

Nonequilibrium dynamics of the ohmic spin-boson model

D.M. Kennes, O. Kashuba, M. Pletyukhov, H. Schoeller, and V. Meden
*Institut für Theorie der Statistischen Physik, RWTH Aachen University and
JARA—Fundamentals of Future Information Technology, 52056 Aachen, Germany*
(Dated: April 14, 2019)

We study the nonequilibrium dynamics of the unbiased, ohmic spin-boson model close to the coherent-to-incoherent transition. In a first setup the system is prepared in a product state. Using complementary renormalization group methods we obtain numerical results for the spin expectation value on all time scales. They are supplemented by an analytical study for intermediate times. In the coherent regime the time evolution for those is characterized by the subtle interplay of damped oscillatory and purely exponential terms. Secondly, we investigate the dynamics when abruptly switching the coupling from a value in the incoherent regime to one in the coherent one. The incoherent dynamics before the quench heavily affects the one after it up to the extent that a critical coupling strength is required to observe nonmonotonic behavior. This exemplifies the importance of non-markovian memory.

PACS numbers: 03.65.Yz, 05.30.-d, 72.10.-d, 82.20.-w

The spin-boson model (SBM) is arguably the most important model used to describe dissipation in small quantum systems coupled to an environment beyond phenomenological approaches. As such it is studied in the context of a variety of distinct fields like condensed matter physics, quantum optics, physical chemistry, and quantum information science [1, 2]. The SBM can be visualized by considering a spin-1/2 in the presence of a Zeeman splitting (bias) ϵ , a tunneling between the two states of amplitude $\Delta \geq 0$, and a coupling λ_k to a bath of bosonic modes with dispersion ω_k . The many-body physics becomes most prominent for bias $\epsilon = 0$ and temperature $T = 0$; we focus on this intriguing parameter regime. The spin-boson coupling is characterized by a spectral density $J(\omega) = \sum_k \lambda_k^2 \delta(\omega - \omega_k)$. Its ω dependence is set by the details of the microscopic model underlying the SBM [1]. It is reasonable to assume that $J(\omega)$ can either be expanded in a Taylor series with the leading term $\sim \omega^s$, $s \in \mathbb{N}$, or is at least a smooth function of this type, with $s > 0$, up to a cutoff ω_c [1, 2]. We concentrate on the ohmic case $s = 1$ which turned out to show particularly rich behavior [1, 2] and exclusively consider the universal physics obtained in the scaling limit with ω_c being much larger than any other energy scale.

In studies of the nonequilibrium dynamics the system is often assumed to be prepared in a product state of spin-up with $P(t=0) = \langle \sigma_z(t=0) \rangle = 1$ and the boson vacuum. The time evolution is performed in the presence of the spin-boson coupling and $P(t)$ asymptotically tends to zero (relaxation protocol). Applying the noninteracting-blip approximation (NIBA) [1] it was argued that for the ohmic SBM with dimensionless coupling $\alpha \geq 0$, where $J(\omega) = 2\alpha\omega\Theta(\omega_c - \omega)$, $P(t)$ changes from being coherent (damped oscillatory) for $\alpha < 1/2$ to incoherent (monotonic decay) for $\alpha > 1/2$. Results of alternative approaches are consistent with this [3–8]. The nonequilibrium dynamics of the SBM in other parameter regimes is discussed in Refs. 9–14. Analytical expressions for $P(t)$

close to the coherent-to-incoherent transition were so far only given for small times $T_K t \ll 1$ [2] and for large ones $(T_K t)^{|1-2\alpha|} \gg 1$ [4], where $T_K = \Delta (\Delta/\omega_c)^{\alpha/(1-\alpha)}$ is the characteristic low-energy scale [1, 2]. Close to the transition $|1-2\alpha| \ll 1$, and the known long-time asymptote [4] is only reached for *exponentially* large times.

We present an analytical result for $P(t)$ at intermediate times. For $\alpha < 1/2$, those are characterized by the interplay of exponentially damped oscillatory behavior and monotonic exponential decay leading to a dynamics very different from the one of the classical example of a damped harmonic oscillator. In fact, our study of this most interesting time regime leads to a new notion of the coherent-to-incoherent transition. We achieve this employing the smallness of $|1-2\alpha|$ and combining the advantages of complementary renormalization group (RG) approaches: functional [15] and the real-time [16] RG.

Our second goal is to understand the dynamics when quenching across the coherent-to-incoherent transition. Recent technological progress to isolate small systems from uncontrolled environmental fluctuations and to manipulate their parameters, e.g. in cold atomic gases, led to a considerable interest in quantum quenches [17]. We prepare the SBM in the initial state of the relaxation protocol and perform the time evolution with a coupling $2\alpha_i - 1 > 0$ (incoherent regime). At $t = t_q$ it is abruptly switched to α_f , with $2\alpha_f - 1 = 1 - 2\alpha_i < 0$ (coherent regime), and the evolution is continued (quench protocol). The incoherent dynamics before the quench heavily affects the one afterwards up to the extent that a critical coupling α_c is required to observe any nonmonotonic behavior in the coherent regime at all. A non-markovian memory term is also important when quenching the other way around as discussed in the Supplementary Material.

Model—The SBM is given by the Hamiltonian

$$H = \frac{\epsilon}{2}\sigma_z - \frac{\Delta}{2}\sigma_x + \sum_k \omega_k b_k^\dagger b_k - \sum_k \frac{\lambda_k}{2}\sigma_z (b_k^\dagger + b_k), \quad (1)$$

with the Pauli matrices σ_ν , $\nu = x, z$ and bosonic ladder operators $b_k^{(\dagger)}$. When using our RG methods we do not directly study this model. Instead we employ the mapping to the interacting resonant level model (IRLM) [1, 2]. In the IRLM a single quantum level of energy ϵ is hybridized with a continuum of spinless fermionic reservoir states ($\epsilon = 0$ corresponds to half dot filling). A fermion occupying the level interacts with the lead states by a Coulomb interaction u . The coupling α of the SBM is related to the dimensionless interaction $U = \rho u$, with the lead density of states ρ (wide band limit), as $1 - 2\alpha = 2U - U^2$ ($U < 0$: incoherent regime, $U > 0$: coherent regime). The point of the coherent-to-incoherent transition $\alpha = 1/2$ thus corresponds to the noninteracting IRLM and is exactly solvable [1, 2]. One furthermore identifies Δ^2/ω_c with the hybridization Γ and ω_c with the leads band width D . The spin expectation value $\langle \sigma_z(t) \rangle$ is given by $2 \langle n(t) \rangle - 1$, with the level occupancy $\langle n(t) \rangle$.

Methods—The functional and real-time RG methods were earlier used to study the nonequilibrium time evolution in the IRLM considering $|\epsilon|/T_K \gg 1$ and a finite voltage applied across the dot [18–20].

The basis of our functional RG approach [15] is the generating functional of the one-particle irreducible vertex functions on the Keldysh contour. In a first step the lead states (IRLM) are integrated out. One then supplements the noninteracting propagation by a cutoff (auxiliary lead cutoff [20]) and takes the derivative with respect to the latter leading to a hierarchy of coupled differential equations for the vertex functions. We truncate it by keeping all terms to leading order in U [20]. From the vertex functions at the end of the flow observables such as $P(t)$ can be computed. Due to the underlying RG procedure the results are way superior to plain perturbation theory—which, in the scaling limit, is plagued by logarithmic terms—and e.g. show the power-law-type renormalization of Δ encoded in the expression for T_K [18]. The flow-equations of the Keldysh components of the self-energy for the dynamics in the relaxation protocol are given in Ref. 20; the ones for the quench protocol with explicitly time-dependent parameters in Ref. 21.

In the complementary real-time RG [16] one focuses on the reduced density matrix of the local system and describes its dynamics in Liouville-Laplace space by

$$P(t) = \frac{i}{2\pi} \int_{-\infty+i0^+}^{\infty+i0^+} dE e^{-iEt} \Pi_1(E), \quad (2)$$

where $\Pi_1(E) = [E + i\Gamma_1(E)]^{-1}$ is an effective propagator and $\Gamma_1(E)$ denotes the energy-dependent charge relaxation rate. The Laplace variable E [22] itself can be used as the flow parameter [23], leading to

$$\frac{d\Gamma_{1/2}(E)}{dE} = -g \Gamma_1(E) \Pi_{2/1}(E), \quad (3)$$

with $g = 2U - U^2$, $\Pi_2(E) = [E + i\Gamma_2(E)/2]^{-1}$, and initial values $\Gamma_n(iD) = \Gamma$. Here, $\Gamma_2(E)/2$ describes the level

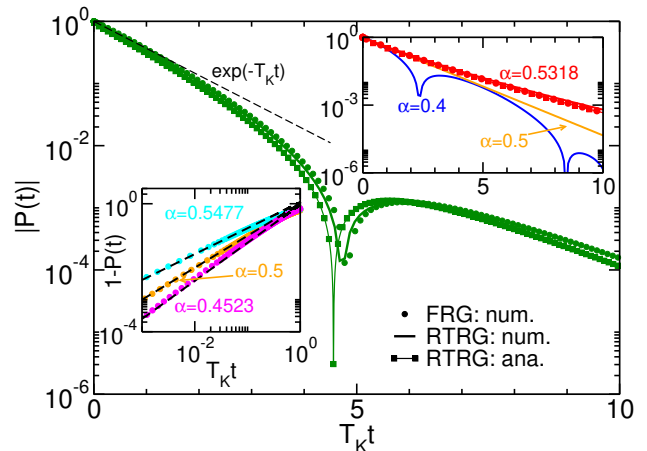


FIG. 1: (Color online) The spin expectation value P of the relaxation protocol as a function of t for different α . Dips correspond to zeros (coherent phase, $\alpha < 1/2$). Main panel: comparison of the full numerical solutions of the functional (F) and real-time (RT) RG flow equations as well as the analytical result Eqs. (6)-(8) for $\alpha = 0.4682$. For $|g \ln t| \ll 1$, $P(t)$ is given by $\exp(-T_K t)$ indicated by the thin dashed line. Right inset: the same as in the main panel for the given α (analytical expression only for $\alpha = 0.5318$; the three curves are barely distinguishable). Left inset: functional RG data for $1 - P(t)$ at short times (dots) and Eq. (4) (dashed lines).

broadening. Solving Eq. (3) offers the unique possibility to identify the singularities of the propagator (poles and branch cuts) in the lower half of the complex plane, from which the individual terms of the time evolution can be identified. The RG equations (3) contain all terms $\mathcal{O}(U \frac{\Gamma}{E})$ and $\mathcal{O}(U^2 \frac{\Gamma}{E})$, such that the exponents of power laws are reliable up to order U^2 [19]. However, some terms $\mathcal{O}(U [\frac{\Gamma}{E}]^2)$ are neglected. This must be contrasted to our functional RG approach, which contains all orders in Γ . To verify that for small $|g|$, that is small $|U|$, considering Eq. (3) is sufficient, we first perform a consistency check by solving the functional and real-time RG equations numerically and computing $P(t)$. In a second step we use Eq. (3) to obtain analytical results.

Relaxation protocol—The main panel and the right inset of Fig. 1 show comparisons of $|P(t)|$ obtained by the numerical solution of the functional and real-time RG equations for different α and an initial product state. The excellent agreement indicates that our real-time RG equations (3) provide a controlled approximation in the limit of small $|1 - 2\alpha| = |g|$. For D (ω_c) sufficiently larger than any other energy scale (scaling limit) $P(t)$ becomes independent of Γ (Δ^2) and D (ω_c) provided $T_K t$ is taken as the argument [24]. The dips in $|P(t)|$ correspond to zeros of $P(t)$ and are characteristic for the coherent regime. For $\alpha = 0.4682$ the ‘oscillatory’ behavior reduces to a single zero at $T_K t \approx 5$, that is no additional zeros are found for times larger than the ones shown in the figure; for decreasing α more zeros might appear, e.g. two for $\alpha = 0.4$

(right inset). The dynamics in the coherent regime of the SBM is thus clearly different from the classical coherent dynamics of a damped harmonic oscillator which would show infinitely many zeros. Before investigating this in more detail we analytically study short times.

Our real-time RG flow equations (3) are only controlled to leading order in g . However, when devising analytical solutions in the different time regimes we keep higher order terms which are produced in the RG flow to solve the equations as accurately as possible. For now we take T_K as our unit of energy, that is $E/T_K \rightarrow E$, $\Gamma_n/T_K \rightarrow \Gamma_n$ and $T_K t \rightarrow t$. We start with small times for which the integral Eq. (2) is dominated by contributions with $|E| \gg \Gamma_1(E)$; we thus approximate $\Gamma_1(E) \approx (-iE)^{-g}$. Expanding the integrand in Eq. (2) gives

$$\begin{aligned} P(t) &\approx \sum_{n=0}^{\infty} \frac{(-1)^n}{2\pi} \int_{-\infty+i0^+}^{\infty+i0^+} dE e^{-iEt} (-iE)^{-1-n(1+g)} \\ &= \sum_{n=0}^{\infty} (-1)^n \frac{t^{n(1+g)}}{\Gamma(1+n[1+g])} \\ \Rightarrow 1 - P(t) &= t^{1+g}/\Gamma(2+g) + \mathcal{O}(t^{2+2g}), \end{aligned} \quad (4)$$

with the Gamma-function $\Gamma(x)$. This result coincides with the one of NIBA (remind that $g = 1 - 2\alpha$) [2]. The short-time behavior of $1 - P(t)$ obtained from the numerical solution of the functional RG equations is shown in the left inset of Fig. 1. The data follow a power law with exponent $2 - 2\alpha$. After expanding the functional RG flow equations for short times they can as well be solved analytically leading to Eq. (4). Neglecting $|g| \ll 1$ in the argument of the Gamma-function in the second line of Eq. (4) one can resum the power series arriving at $P(t) \approx \exp(-t^g t)$. For $|g \ln t| \ll 1$ we can set $t^g \approx 1$, thus $P(t) \approx e^{-t}$; for such t the data in the main panel of Fig. 1 indeed approximately follow an exponential decay with rate 1 (that is T_K , after reintroducing it).

When analytically computing $P(t)$ for $t \gtrsim 1$ using real-time RG one has to separately consider the branch-cut contribution to the integral Eq. (2) for all g and the pole contributions for $g \geq 0$. The former follows from the branch cut of $\Gamma_1(E)$ on the imaginary axis starting at the pole $-i\Gamma_2^*/2$ of $\Pi_2(E)$. Taking $\Gamma_2(E) \approx \Gamma_2^*$ in $\Pi_2(E)$, we get $\Gamma_1(E) \approx (\Gamma_2^*/2 - iE)^{-g}$ from Eq. (3), leading to

$$P_{bc}(t) = -\frac{e^{-\Gamma_2^* t/2}}{\pi} \int_0^{\infty} dx \operatorname{Im} \left\{ \frac{e^{-xt}}{\frac{\Gamma_2^*}{2} + x - e^{i\pi g} x^{-g}} \right\}. \quad (5)$$

Replacing x^g by t^{-g} in the denominator gives a very good approximation for $t \gtrsim 1$. The integral can then be expressed in terms of the exponential integral E_1 as

$$P_{bc}(t) \approx \frac{1}{\pi} \operatorname{Im} \left\{ e^{-\gamma t} E_1 \left(\left[\frac{1}{2} \Gamma_2^* - \gamma \right] t \right) \right\}, \quad \gamma = e^{-i\pi g} t^g. \quad (6)$$

A comparison with the numerical solution shows that to find the pole positions $z_1 = \pm\Omega - i\Gamma_1^*$ ($z_2 = -i\Gamma_2^*/2$)

of $\Pi_1(E)$ ($\Pi_2(E)$) one can set $\Gamma_1(E) \approx \Gamma_2(E) \approx iz_1$ ($\Gamma_1(E) \approx \Gamma_2(E) \approx \Gamma_2^*$) in $\Pi_n(E)$. The RG equations can then be solved analytically leading to

$$\Gamma_2^* \approx 2 \left[\frac{\pi g}{2 \sin(\pi g)} \right]^{\frac{1}{1+g}}, \quad \Omega + i\Gamma_1^* \approx e^{(i\pi + \ln 2) \frac{g}{1+g}}, \quad (7)$$

as well as to the residuum $(1-g)/(1+g)$ of $\Pi_1(E)$ at the pole z_1 . Using this, the pole contribution becomes

$$P_p(t) \approx 2 \frac{1-g}{1+g} \cos(\Omega t) e^{-\Gamma_1^* t} \Theta(g). \quad (8)$$

The sum of Eqs. (6) and (8) supplemented by the parameter dependencies of the rates $\Gamma_{1/2}^*$ and the frequency Ω Eq. (7) constitutes our analytical result for $P(t)$ at times $t \gtrsim 1$ [25]. As exemplified in Fig. 1 ($\alpha = 0.4682$; main panel) it shows excellent agreement with the numerical solution of the RG flow equations. The position of the zeros of $P(t)$ sensitively depends on the approximations leading to the analytical result. Any inconsistency will easily move their location by several T_K^{-1} . The agreement is even better for $\alpha > 1/2$ ($\alpha = 0.5318$, right inset).

For $\alpha < 1/2$ a pole contribution of the above type also appears in NIBA [1, 2] and in conformal field theory [5]. Our ratio Ω/Γ_1^* Eq. (7) coincides with the one obtained by these methods [26, 27]. While no branch-cut contribution appears in the conformal field theory study [5] the one of NIBA leads to a purely algebraic decay which turned out to be an artifact of this approximation [2]. In Ref. 4 NIBA was improved leading to

$$P_{bc}(t) = -g[1 + 3\Theta(-g)] \frac{e^{-t/2}}{t^{1+|g|}}. \quad (9)$$

This result coincides with our Eq. (6) evaluated for $t^{|g|} \gg 1$ and taking into account that $\Gamma_2^* \approx 1$ (that is T_K , after reintroducing it) up to higher order corrections. For such times also the functional RG equations can be solved analytically leading to Eq. (9). We emphasize that for $\alpha < 1/2$ the sum of the pole contribution Eq. (8) and the asymptotic result Eq. (9) does not give a meaningful approximation to the dynamics for the times shown in Fig. 1 for which the coherent and incoherent parts are comparable and nonmonotonic ('oscillatory') behavior is found. For those it is crucial to keep the branch-cut term in the form of Eq. (6) with the exponential integral [28].

Quench protocol—In Fig. 2 we show $P(t)$ when, after some evolution in the incoherent regime (for $0 \leq t \leq t_q$, not shown in Fig. 2; see Fig. 1), the coupling is abruptly quenched to the coherent one with $2\alpha_f - 1 = 1 - 2\alpha_i < 0$. The two different couplings α_i and α_f lead to the two characteristic scales T_K^i and T_K^f , which in the scaling limit differ by orders of magnitude. Therefore the model parameters Γ (Δ^2) and D (ω_c) cannot be scaled out as efficiently as in the relaxation protocol (see below). To minimize the influence of the transient dynamics before

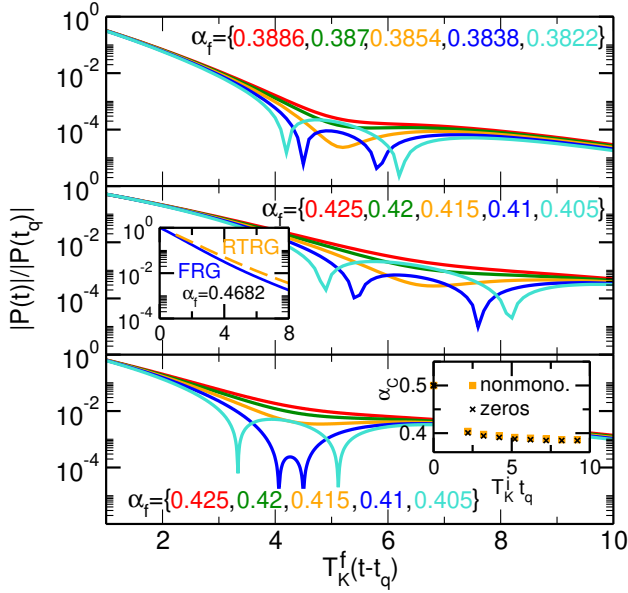


FIG. 2: (Color online) The spin expectation value P of the quench protocol as a function of t for different α close to α_c . The scaling limit is realized by $\Gamma/D = 1/200^2$. Upper panel: numerical solution of functional RG equations. Central panel: numerical solution of real-time RG equations. Lower panel: analytical result Eq. (11). The times are restricted to $t > t_q$; for $0 < t < t_q$, see Fig. 1. Left inset: comparison of numerical functional and real-time RG data for α close to $1/2$. Right inset: dependence of α_c on the time $T_K^i t_q$ the evolution was performed in the incoherent regime (functional RG data). Two different definitions of α_c are compared. In the first α_c is defined as the α_f at which the first zero of $P(t)$ can be observed, in the second as the α_f at which the curve first shows a nonmonotonicity. The two values barely differ.

the quench we consider $T_K^i t_q$ between 5 and 10. In the left inset we compare the data obtained by the numerical solution of the functional [21] and real-time RG equations (for details of the latter, see below). The agreement for $\alpha_{i/f}$ close to $1/2$ is excellent. Even though the same coupling $\alpha_f = 0.4682$ as in the main panel of Fig. 1 is considered the data for the quench dynamics displayed in the left inset of Fig. 2 are monotonic; no indications of coherent behavior are found. The incoherent dynamics before the quench thus heavily affects the one afterwards. The memory persists over several $1/T_K^f$, with T_K^f entering the rates for $t > t_q$. To further investigate this, results for smaller α_f are shown in the upper (functional RG) and central (real-time RG) panel. Nonmonotonic (‘oscillatory’) behavior can only be found for α_f being smaller than some critical coupling α_c . As $|1 - 2\alpha_c| \ll 1$ does not hold strictly, our two approximate RG methods give values for α_c which differ by a few percent. Its precise value can only be obtained using a method which treats higher order contributions consistently. The right inset shows that α_c does only weakly depend on t_q and quickly saturates for $T_K^i t_q \gtrsim 5$.

Quenches have so far not been studied using real-time

RG; the technical details will be given elsewhere. In this approach the memory of the spin state is preserved in the excitations of the bath. Classifying the memory contributions by the number of lead excitations (of the IRLM Hamiltonian) that have gone through the quench one can show that the terms with n excitations are proportional to $A^n = (T_K^i/T_K^f)^{n/2} \approx (\Gamma/D)^{n|g_f|}$, with $A \ll 1$. Restricting ourselves to the case of a single excitation with Matsubara frequency Λ we get ($t' = t - t_q \geq 0$)

$$P(t') = P^f(t')P^i(t_q) - g_i \int_0^\infty d\Lambda F_\Lambda^f(t') F_\Lambda^i(t_q), \quad (10)$$

$$F_\Lambda^\kappa(t) = - \int_{-\infty}^\infty \frac{dE}{2\pi} e^{-iEt} \Pi_1^\kappa(E + i\Lambda) \sqrt{\Gamma_1^\kappa(E)} \Pi_2^\kappa(E)$$

with $\kappa = i, f$ and $P^\kappa, \Gamma_{1/2}^\kappa$ computed as in the relaxation protocol with the corresponding $\alpha_{i/f}$ and initial condition $P^\kappa(0) = 1$. The first term describes standard relaxation while the second memory term implies (dissipative) non-markovian dynamics. It has no analog for quenches in closed systems. The data in the central panel and in the upper inset of Fig. 2 were obtained by numerically performing the E and Λ integrals in Eq. (10) on the basis of the numerical solution of Eq. (3). Fixing D the results depend only very weakly on Γ (via A) [29]. To gain qualitative analytical insight of the interplay of the relaxation dynamics and the non-markovian correction we evaluate the integrals keeping only the terms which dominate for $|g_{i/f}| \ll 1$. The result

$$\frac{P(t')}{P(t_q)} \approx 2(1 - A)e^{-\Gamma_1^{*f} t'} \cos(\Omega^f t') + Ae^{-\Gamma_2^{*f} t'/2} \quad (11)$$

is shown in the lower panel of Fig. 2. The memory generates a coherent and an incoherent contribution $\propto A$. The first has a negative sign and suppresses the coherent part while the second enhances the incoherent term compared to the one of the relaxation protocol; for $g_f \ll 1$ the latter is subdominant and thus not written in Eq. (11). This explains the appearance of a critical α_c .

In the Supplementary Material we show that a dominant non-markovian memory term can also appear when quenching from the coherent into the incoherent regime. This way it is possible to transfer nonmonotonic behavior deep into the incoherent regime.

Summary—Our comprehensive study of the nonequilibrium time evolution of the unbiased, ohmic spin-boson model out of a product state shows that the time evolution close to the coherent-to-incoherent transition is significantly different from the one of a classical damped harmonic oscillator close to its corresponding transition. In the coherent regime and for intermediate times damped oscillatory terms compete with monotonic exponential ones; a subtle interplay captured by our analytical result. When quenching from the incoherent to the coherent regime the coherent (‘oscillatory’) dynamics is fragile and disappears for couplings close to but smaller than

1/2. This exemplifies the importance of non-markovian memory.

Acknowledgments—This work was supported by the DFG via FOR 723. We thank R. Egger and U. Weiss for comments on an earlier version of this paper.

-
- [1] A.J. Leggett, S. Chakravarty, T.A. Dorsey, M.P.A. Fisher, A. Garg, and W. Zwerger, *Rev. Mod. Phys.* **59**, 1 (1987).
- [2] U. Weiss, *Quantum Dissipative Systems* (World Scientific Publishing Company, Singapore, 2012).
- [3] R. Egger and C.H. Mak, *Phys. Rev. B* **50**, 15210 (1994).
- [4] R. Egger, H. Grabert, and U. Weiss, *Phys. Rev. E* **55**, R3809 (1997).
- [5] F. Lesage and H. Saleur, *Phys. Rev. Lett.* **80**, 4370 (1998).
- [6] F.B. Anders and A. Schiller, *Phys. Rev. B* **74**, 245113 (2006).
- [7] H. Wang and M. Thoss, *New J. Phys.* **10**, 115005 (2008).
- [8] P.P. Orth, A. Imambekov, and K. Le Hur, *Phys. Rev. A* **82**, 032118 (2010).
- [9] M. Grifoni and P. Hänggi, *Phys. Rep.* **304**, 229 (1998).
- [10] M. Keil and H. Schoeller, *Phys. Rev. B* **63**, 180302 (2001).
- [11] D.P. DiVincenzo and D. Loss, *Phys. Rev. B* **71**, 035318 (2005).
- [12] A. Hackl and S. Kehrein, *Phys. Rev. B* **78**, 092303 (2008).
- [13] A. Alvermann and H. Fehske, *Phys. Rev. Lett.* **102**, 150601 (2009).
- [14] P.P. Orth, D. Roosen, W. Hofstetter, and K. Le Hur, *Phys. Rev. B* **82**, 144423 (2010).
- [15] W. Metzner, S. Salmhofer, C. Honerkamp, V. Meden, and K. Schönhammer, *Rev. Mod. Phys.* **84**, 299 (2012).
- [16] H. Schoeller, *Eur. Phys. J. Spec. Top.* **168**, 179 (2009).
- [17] A. Polkovnikov, K. Sengupta, A. Silva, and M. Vengalattore, *Rev. Mod. Phys.* **83**, 863 (2011).
- [18] C. Karrasch, S. Andergassen, M. Pletyukhov, D. Schuricht, L. Borda, V. Meden, and H. Schoeller, *Europhys. Lett.* **90**, 30003 (2010).
- [19] S. Andergassen, M. Pletyukhov, D. Schuricht, H. Schoeller, and L. Borda, *Phys. Rev. B* **83**, 205103 (2011); **84**, 039905(E) (2011).
- [20] D.M. Kennes, S.G. Jakobs, C. Karrasch, and V. Meden, *Phys. Rev. B* **85**, 085113 (2012).
- [21] D.M. Kennes and V. Meden, *Phys. Rev. B* **85**, 245101 (2012).
- [22] Note that we use the definition $f(E) = \int_0^\infty e^{iEt} f(t)$ for the Laplace transform.
- [23] M. Pletyukhov and H. Schoeller, *Phys. Rev. Lett.* **108**, 260601 (2012).
- [24] The scaling limit is treated consistently in numerical studies within the functional and the real-time RG by using the definition $T_K = -\pi/(2\chi)$, with the charge susceptibility χ , instead of the analytical expression for T_K given above. Both agree to leading order in $g = 1 - 2\alpha$.
- [25] For $g \rightarrow 0$ the integral Eq. (5) gives $P_{bc} = -e^{-t}$ which must be added to $P_p = 2e^{-t}$ leading to the exact result $P(t) = e^{-t}$.
- [26] Note that the g of Ref. 5 corresponds to our α .
- [27] The prefactor of the pole contribution Eq. (8) agrees with the one of NIBA only to order g^0 ; we find a deviation by a factor of 2 in the linear term [1, 2]. We were informed by U. Weiss that computing it within improved NIBA [4]—which was not done in this reference—gives a result which agrees to ours up to first order.
- [28] The expansion of the exponential integral in Eq. (6) for large arguments leads only to an asymptotic series, which in the time regime of interest cannot be truncated in a consistent way.
- [29] Varying $\Gamma/D \sim \Delta^2/\omega_c^2$ by an order of magnitude around the average value $2.5 \cdot 10^{-5}$ results in a change of α_c by only a few percent.

Nonequilibrium dynamics of the ohmic spin-boson model Supplementary Material

D.M. Kennes, O. Kashuba, M. Pletyukhov, H. Schoeller, and V. Meden
*Institut für Theorie der Statistischen Physik, RWTH Aachen University and
JARA—Fundamentals of Future Information Technology, 52056 Aachen, Germany*

We here provide further evidence for the importance of non-markovian memory in the quench dynamics of the unbiased ohmic SBM. To this end we study a second quench protocol which is opposite to the first one investigated in the main text. The system is initially prepared in the standard product state. Up to t_q the time evolution is performed with α_i taken from the coherent regime, $2\alpha_i - 1 < 0$. At t_q the coupling is quenched to α_f , with $2\alpha_f - 1 = 1 - 2\alpha_i > 0$ from the incoherent regime. Considering a sufficiently large $T_K^i t_q$ we minimized the influence of the transient dynamics in the first quench protocol; up to an overall scaling factor $P(t)$ after the quench very quickly becomes independent of the quench time when increasing $T_K^i t_q$. In the second quench protocol the situation is more complex. To keep the discussion transparent we focus on α_i 's close to $1/2$ for which only a single zero at time t_0 is found in the relaxation protocol. The behavior after the quench sensitively depends on $t_q - t_0$. In Fig. S1 we show $|P(t)|$ obtained from the numerical solution of the functional as well as the real-time RG equations for the second quench protocol. The coupling α_i is fixed at 0.4682 as already used in the main text. In the relaxation protocol $T_K t_0 \approx 5$ for this coupling (see Fig. 1 as well as the curve with $t_q > t_0$ in Fig. S1). Different quenching times t_q are considered as indicated by the vertical dotted lines. For $t_q > t_0$ the dynamics at times larger than t_q very quickly adapts to the new rate $\approx T_K^f/2$ of the incoherent dynamics [see Eq. (9) and the dashed line in Fig. S1] and is similar to the large time behavior of the relaxation protocol with $\alpha = \alpha_f$. We reemphasize that in the scaling limit T_K^f is orders of magnitude smaller than T_K^i . In Fig. S1 the x -axis scale is therefore switched from $T_K^i t$ to $T_K^f t$ at the respective t_q . The behavior is significantly different for $t_q < t_0$. In this case nonmonotonic ('oscillatory') behavior is found for times $t > t_q$ at which the time evolution is performed with $\alpha_f = 0.5318 > 1/2$ taken from the incoherent regime. The smaller $t_q - t_0$ the further into the incoherent regime the zero of $P(t)$ can be transferred. As in the first quench protocol this memory persists over several $1/T_K^f$ (roughly $10/T_K^f$ for the smallest $t_q - t_0$ considered in the figure), with T_K^f determining the rates after the quench. We note in passing that the functional and

real-time RG data again show excellent agreement. The analytical result Eq. (11) was specifically developed for the first quench protocol and cannot be used for the second one. Analytical results for the latter will be given elsewhere.

To show that the transfer of nonmonotonic coherent behavior deep into the incoherent part of the dynamics is indeed given by a non-markovian memory term [see Eq. (10)]—and not by the more trivial effect of modified initial conditions for the incoherent dynamics at t_q resulting out of the relaxation dynamics for $t < t_q$ —we artificially switch off this term in our RG calculations. As shown in the inset of Fig. S1 the zero of $P(t)$ vanishes in the absence of the memory term. This indicates that the appearance of the zero is exclusively coded in the history of the dynamics and not in the values of the systems density matrix at a selected time.

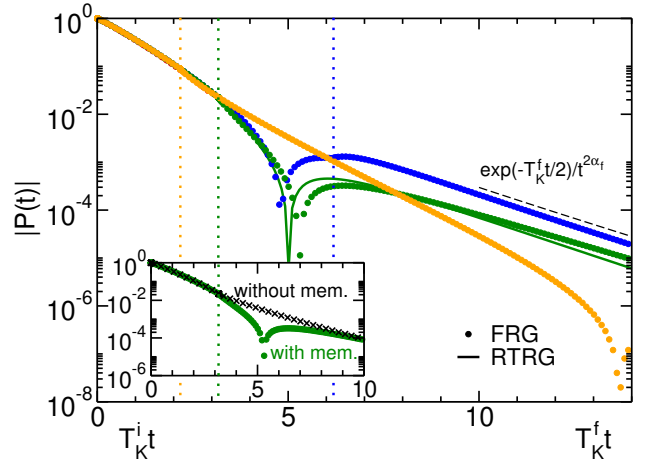


FIG. S1: (Color online) The spin expectation value P of the second quench protocol as a function of t for $\alpha_i = 0.4682$ and different quench times t_q (indicated by the vertical dotted lines). At the respective t_q the x -axis scale is switched from $T_K^i t$ to $T_K^f t$. Main panel: data of the numerical solutions of the functional and real-time RG flow equations. The thin dashed line is an exponential term with rate $T_K^f/2$ and a subleading power-law correction. Inset: functional RG data with and without the memory term.